Singlet Oxygen Generation from Polymer Nanoparticles–Photosensitizer Conjugates Using FRET Cascade

ARTICLE *in* THE JOURNAL OF PHYSICAL CHEMISTRY C · APRIL 2014

Impact Factor: 4.77 · DOI: 10.1021/jp4127094

4 AUTHORS, INCLUDING:

Santanu Bhattacharyya
Ludwig-Maximilians-University of Munich
26 PUBLICATIONS **195** CITATIONS
SEE PROFILE

Avijit Baidya
Indian Institute of Technology Madras
1 PUBLICATION **9** CITATIONS
SEE PROFILE

Amitava Patra
Indian Association for the Cultivation of Science
172 PUBLICATIONS **4,138** CITATIONS
SEE PROFILE

THE JOURNAL OF PHYSICAL CHEMISTRY C

Article

pubs.acs.org/JPCC

Singlet Oxygen Generation from Polymer Nanoparticles–Photosensitizer Conjugates Using FRET Cascade

Santanu Bhattacharyya, Monoj Kumar Barman, Avijit Baidya,† and Amitava Patra*

Department of Materials Science, Indian Association for the Cultivation of Science, Kolkata 700 032, India

Supporting Information

ABSTRACT: Herein, we demonstrate π-conjugated polymer nanoparticles–photosensitizer conjugates for singlet oxygen generation via FRET cascade, which would be useful for photodynamic therapy. Rose Bengal (RB) molecules are attached on the surface of coumarin 153 (C153)-dye-doped poly[*N*-vinyl carbazole] (PVK) polymer nanoparticles, where polymer nanoparticles act as efficient light-absorbing antenna materials. The energy funneling from C153 to RB at the excitation of the PVK host (340 nm) is confirmed by shortening of decay time of C153 and disappearing of its rise time. Again, it is evident that the efficient multistep energy transfer occurs from host PVK to RB dye molecules through C153 dye molecules to generate singlet oxygen ($^1O_2$) in solution. In addition, photo-oxidation of 2-chlorophenol provides quantitative evidence of singlet oxygen generation in different systems indirectly. The estimated singlet oxygen quantum yield for RB-attached C153-dye-doped PVK polymer nanoparticles is 21%. The present investigations should pave the way for future development of different photodynamic and theranostic devices.

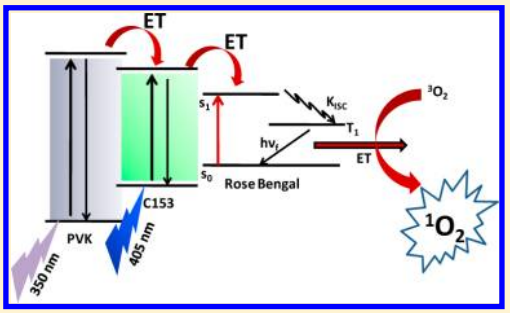

INTRODUCTION

Great importance has been given to the design of a photosensitizer molecule for cancer treatment by using photodynamic therapy (PDT). In photodynamic therapy, light is being used to activate the photosensitizer for producing singlet oxygen, which can destroy cancer cells.[1−3] Currently, rare-earth-doped upconverted nanoparticles are being investigated for multiphoton photodynamic therapy because of several advantages (i.e., NIR light excitation, greater penetration into tissue, and less tissue damange).[5−7] Furthermore, semiconducting QDs are also found to be suitable for photodynamic therapy because of their broad absorption cross section, sharp emission spectra, comparatively higher QYs, and better photostability.[8,9] Samia et al. demonstrated that CdSe QDs can be used to sensitize phthalocyanine (Pc4) via a resonance energy transfer to generate singlet oxygen for PDT applications.[10] Hsieh and his co-workers have designed an iridium complex−CdSe/ZnS QD system to produce a high quantum yield of singlet oxygen where the Ir complex is being used as a sensitizer.[11] Shi et al. have demonstrated a water-soluble CdTe QDs−photosensitizer system for this purpose.[12] Peptide-coated QD−photosensitizer conjugates for generation of a high quantum yield (31%) of singlet oxygen has been reported.[13] Singlet oxygen is being generated in these systems by resonance energy transfer from QD to photosensitizer molecules. Recently, Charron et al. have nicely demonstrated the FRET-based photosensitization mechanism of chlorine e6 by InP/ZnS core−shell QDs.[14] However, the QD-based system for photodynamic therapy has several disadvantages, including power law blinking, toxicity due to heavy metals, and a solubility problem in water.[15]

Thus, semiconducting π-conjugated polymer nanoparticles are a promising alternative for this purpose because of their tunable photoemission, comparatively higher brightness, easy synthesis procedures, lower toxicity, and greater photostability.[16,17] The luminescent behavior can also be enriched by doping of the fluorescent dye molecules inside the polymer nanoparticles.[18−24] In addition, due to large absorption cross section of semiconducting conjugated polymer NPs, they can be applied for the photosensitization of different photosensitizer (PS) molecules. Here, conjugated polymers in their nanoparticle form can act as efficient light antenna materials which strongly absorb light and photosensitize the PS molecules by an efficient FRET process followed by $^1O_2$ generation.[25−27] Very recently, Shen and his co-workers have synthesized conjugated polymer nanoparticles from tetraphenylporphyrin (TPP)-doped poly[9,9-dibromohexyl-fluorene-2,7-ylenethylene-*alt*-1,4-(2,5-dimethoxy)phenylene] (PFEMO) by using the reprecipitation method.[28] They have demonstrated the efficient intraparticle energy transfer from PFEMO to TPP by two-photon excitation, which enhances the singlet oxygen generation efficiency. Furthermore, McNeill and his co-workers have described the photosensitization of organic PS molecules inside polyfluorene nanoparticles having a large absorption cross section of multiphoton excitation.[29]

In this work, we design a system where Rose Bengal (RB) dye molecules are attached with the surface of C153-dye-doped PVK polymer nanoparticles. We investigate the photosensitiza-

Received: December 28, 2013
Revised: March 11, 2014
Published: April 15, 2014

tion of RB dye molecules due to both FRET cascade from PVK to surface-attached RB dye molecules through encapsulated C153 dye molecules and a direct FRET process from encapsulated C153 to RB molecules. Finally, singlet $^1O_2$ generation has been indirectly proved by the photo-oxidation of 2-chlorophenol in D_2O medium. Results show the clear effect of encapsulated C153 dye molecules on the amount of $^1O_2$ generation followed by photo-oxidation of 2-chlorophenol.

MATERIALS

PVK [Poly(9-vinylcarbazole)] (Aldrich), coumarin 153 (C153) (Sigma-Aldrich), Rose Bengal (RB) dye (Aldrich), distilled tetrahydrofuran (Aldrich), polyetheleneimine (Aldrich, M_w of 1800), deionized water (MERCK), NaN_3 (99% Fluka), and imidazole (Aldrich) were used as received for our synthesis in the present study.

EXPERIMENTAL PROCEDURES

In our work, 0.8 wt % C153-doped PVK polymer nanoparticles (SEM image is given in Figure S1A, Supporting Information) have been synthesized by typical reprecipitation method described previously.[22,30] The surface charges of polymer nanoparticles were investigated by Zeta-potential measurements using a Zetasizer nanosystem (Malvern Instrument Ltd.) at room temperature. The average zeta potential data of C153-doped PVK polymer nanoparticles was (−) 35 mV.[31] Therefore, to increase the interactions of anionic RB dye molecules on the surface of polymer nanoparticles, it is very important to convert negatively charged polymer nanoparticles into positive charged surface. We have used cationic polyelectrolyte PEI (polyetheleneimine) for the surface charge modification of semiconducting dye-encapsulated polymer nanoparticles. The surface charge of PEI-modified C153-doped PVK polymer nanoparticles became positive (+25 mV). Excess RB dye molecules have been removed by dialysis, having a molecular cutoff of 12−14 kDa. After addition of the RB dye molecules on the PVK nanoparticle surface, the Zeta potential data converted to −4 mV. It suggests that the electrostatic attachment of RB on the positive charge surface of C153-doped PVK polymer nanoparticles. All the zeta potential curves are given in Supporting Information Figure S2. The concentration of Rose Bengal was varied from 0 to 1.05×10^{-6} M.

The morphological characterization of dye-doped PVK nanoparticles was performed by field emission scanning electron microscopy (FESEM, JEOL, JSM-6700F). Room temperature optical absorption spectra were taken by a UV−vis spectrophotometer (Shimadzu). Room temperature photoluminescence spectra were taken by a Fluoromax-P (Horiba JOBIN YVON) photoluminescence spectrophotometer. In TCSPC measurement, we have used picosecond NANO-LED IBH-340 and IBH-405 L for 340 and 405 nm wavelength of excitation, respectively. All emission decay data were convoluted with the cross-correlation signal and fitted to a multiexponential function using DAS-6 software by using the following:[32]

$$P(t) = b + \sum_i^n \alpha_i \exp\left(-\frac{t}{\tau_i}\right) \quad (1)$$

Here, n is the number of emissive species, b is the baseline correction ("dc" offset), and α_i and τ_i are the pre-exponential factors and excited state fluorescence lifetimes associated with the i^{th} component, respectively. The average lifetime, $<\tau>$, was calculated from the following formula,[32]

$$<\tau> \sum_i^n \alpha_i \tau_i^2 / \sum_i^n \alpha_i \tau_i \quad (2)$$

The phosphorescence spectra of $^1O_2$ was monitored by using a Fluorolog-3 IHR spectrafluorometer (Jobin-Yvon) equipped with a NIR sensitive photomultiplier (Hamamatsu model: R5509-72) operated at a temperature of 273 K. Photo-oxidation of 2-chlorophenol was made by using a 300 W xenon lamp, and a cutoff filter of 350 nm has been used to avoid the self-degradation of 2-chlorophenol. All the photo-oxidation measurements have been done at pH 7 in D_2O medium.

RESULTS AND DISCUSSION

Steady-State Spectroscopy. FE-SEM images (depicted in Figure S1) and dynamic light scattering studies (depicted in Figure S3) suggest that surface-attached RB dye molecules do not affect the morphological features of C153-doped PVK NP. Before and after electrostatic attachment of RB dye molecules on the C153-doped PVK NP surface, the particle size remains constant (~100 nm in diameter). It indirectly proves that RB dye molecules are basically on the surface of the NP, and it does not alter molecular packing of PVK NP. UV−vis absorption spectroscopy (depicted in Figure 1) is used to investigate the ground state electronic interactions of C153-doped PVK polymer nanoparticles with surface-attached RB dye molecules. The absorption peak at 345 nm is observed for PVK nanoparticles (Figure 1a), which is due to their $\pi-\pi^*$ transition.[33] The absorption band of PVK remains unchanged except a small peak at 420 nm after incorporation of 0.8 wt % of C153 molecules inside the PVK polymer nanoparticles (Figure 1b). The absorption peak at 549 nm with a shoulder at 511 nm is observed (Figure 1c) for aqueous solution of Rose Bengal (RB) molecules (1.05×10^{-6} M). However, the absorption peaks of RB dye molecules are red-shifted and broaden after attachment with the PVK polymer nanoparticle surface (Figure 1d). The peak at 549 nm is shifted to 563 nm, and the peak at

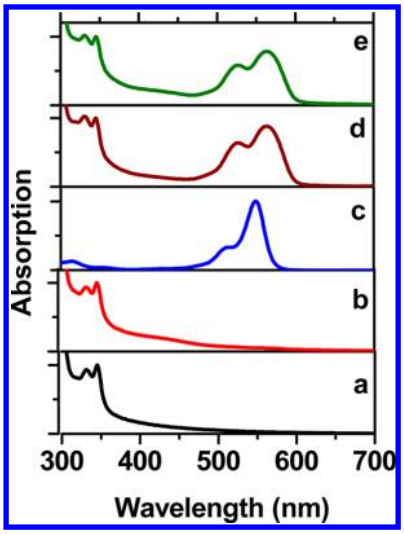

Figure 1. UV−vis absorption spectra of (a) pure PVK NP, (b) C153-doped PVK NP, (c) pure RB in water, (d) PVK NP + RB, (e) C153-doped PVK NP + RB.

dx.doi.org/10.1021/jp4127094 | J. Phys. Chem. C 2014, 118, 9733−9740

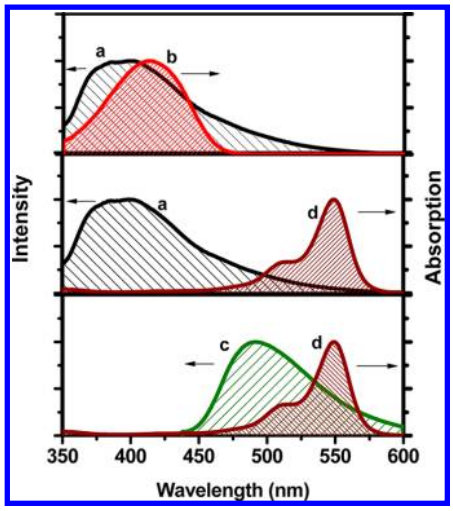

Figure 2. Spectral overlap between the (a) emission spectra of PVK NP and (b) absorption spectra of C153 (upper panel). Spectral overlap between the (a) emission spectra of PVK NP and (d) absorption spectra of RB (middle panel). Spectral overlap between the (c) emission spectra of C153 and (d) absorption spectra of RB (lower panel).

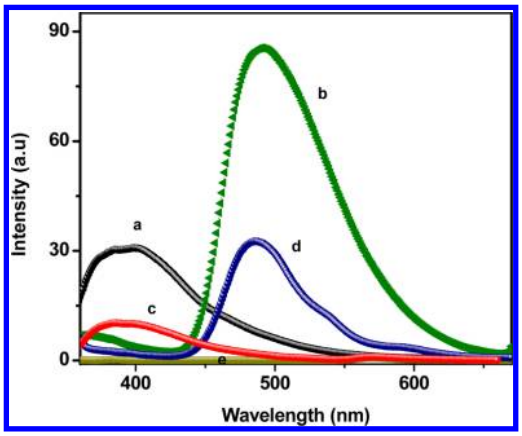

Figure 3. Photoluminescence spectra of pure PVK NP (a), C153-doped PVK NP (b), PVK NP + RB (c), C153-doped PVK NP + RB (d), pure RB in water (e). (λ_{em} = 340 nm).

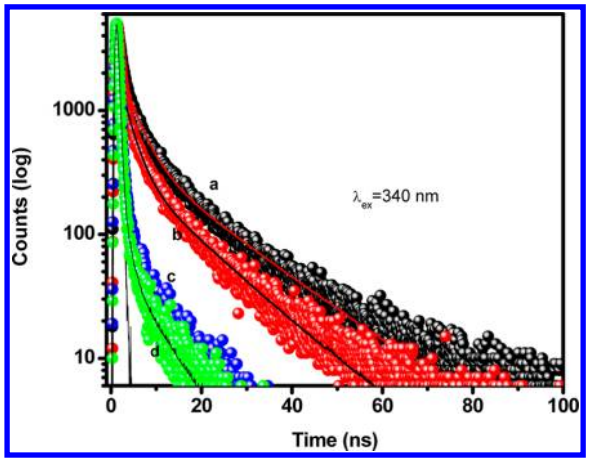

Figure 4. Emission decay curves of pure PVK NP (a), PVK NP + RB (b), C153-doped PVK NP (c), C153-doped PVK NP + RB (d). (λ_{em} = 400 nm).

511 nm is shifted to 526 nm after attachment. Relative optical density ratio between lower wavelength absorption maxima (λ_1) and higher wavelength absorption maxima (λ_2) (i.e., λ_1/λ_2) indicates the extent of aggregation of RB dye molecules.[34] In the case of free RB in water, λ_1/λ_2 is 0.33, which indicates the monomeric RB dye molecules in water at our chosen concentration (1.05×10^{-6} M). After electrostatic attachment on positive-surface-charge PVK NP, the λ_1/λ_2 value increases noticeably up to 0.72 (see Supporting Information Figure S4A), because the PVK NP surface acts as a template where RB dye molecules reside in close proximity and form an aggregation.[34] In addition, the emission peak maxima of RB is shifted from 569 to 589 nm after their electrostatic attachment on the PVK NP surface (Figure S4B). It further supports the aggregation of RB on the PVK NP surface. Furthermore, the calculated quantum yields of RB are 0.010 and 0.004 for free dye in water and the surface-attached system, respectively. It further supports the aggregation of RB dye molecules on the positively charged surface of PVK NP. In the case of RB dye in water, the calculated molar extinction coefficient is 8.4×10^4 M^{-1} cm^{-1} at 549 nm (peak maxima). After electrostatic attachment with the PVK NP surface, the molar extinction coefficient of RB became 4.8×10^4 M^{-1} cm^{-1} at 563 nm (peak maxima). Furthermore, the molar extinction efficient of dye-doped PVK NP is 1.3×10^7 M^{-1} cm^{-1} (considering the particle concentration ~80 nM reported previously).[24] The comparatively higher molar extinction coefficient of PVK NP should help to absorb a large extent of incident light and to efficiently photosensitize the surface-attached RB dye molecules through multistep energy transfer phenomena. Furthermore, it is to be noted that the overall absorption spectrum (Figure 1e) covers almost the whole visible range (from 350 to 600 nm) in the case of RB-attached C153-doped PVK polymer nanoparticles. Thus, the photoexcitation wavelength can be varied from 350 to 600 nm for photosensitization of RB.

It is shown in Figure 2 that there is a good spectral overlap between the emission spectrum of PVK polymer nanoparticle with the absorption spectrum of encapsulated C153 and surface-attached RB dye molecules, as a result of the broad emission spectrum of PVK nanoparticles. The overlap integrals in all cases are calculated by using the following equation[32]

$$J(\lambda) = \int_0^\infty F_D(\lambda)\varepsilon_A(\lambda)\lambda^4 d\lambda / \int_0^\infty F_D(\lambda) d\lambda \quad (3)$$

where F_D (λ) demonstrates the integrated area of donor emission in a particular wavelength range, and ε_A represents the wavelength-dependent molar extinction coefficient of acceptor molecules. The calculated overlap integral values are 1.92×10^{15} M^{-1} cm^{-1} nm^4 and 4.88×10^{14} M^{-1} cm^{-1} nm^4 between the emission spectra of PVK nanoparticles and the absorption spectrum of C153 and RB dye molecules, respectively. The overlap integral value between the emission spectrum of encapsulated C153 and the absorption spectrum of surface-attached RB dye molecules is 2.6×10^{15} M^{-1} cm^{-1} nm^4. Results indicate that there is a possibility of multistep energy transfer from donor PVK nanoparticles to encapsulated C153 dye molecules and the surface attached RB dye molecules. In addition, the multistep FRET cascade process from host PVK to surface-attached RB molecules through encapsulated C153 dye molecules would be possible. Further discussion has been carried out later in this manuscript.

Figure 3 shows the photoluminescence spectra of PVK NP, C153-doped PVK NP, and with and without surface-attached

dx.doi.org/10.1021/jp4127094 | J. Phys. Chem. C 2014, 118, 9733−9740

Table 1. Emission Decay Parameters of PVK NP in Different Conditions (λ_{ex} = 340 nm)

sample	λ_{em} (nm)	τ_1 (ns) a_1	τ_2 (ns) a_2	τ_3 (ns) a_3	<τ> (ns)
PVK NP	400	3.31 (0.11)	16.24 (0.025)	0.28 (0.865)	1.01
PVK NP + RB	400	2.5 (0.05)	13.21 (0.01)	0.16 (0.94)	0.40
C153-doped PVK NP	390	1.45 (0.003)	0.10 (0.99)	7.87 (0.0004)	0.11
C153-doped PVK NP + RB	390	1.47 (0.001)	0.69 (0.99)	7.92 (0.0002)	0.069

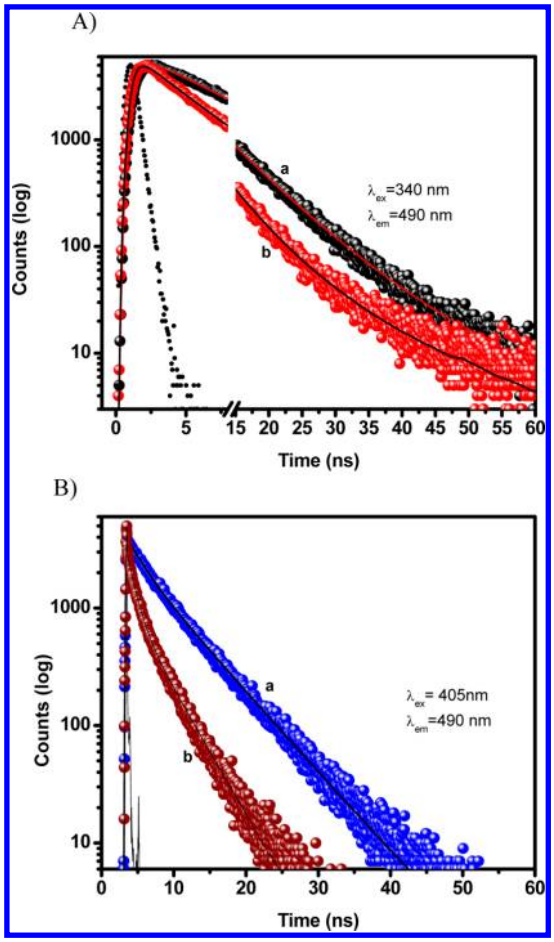

Figure 5. Emission decay curves of C153 encapsulated in PVK NP without (a) and with (b) surface-attached RB at 340 nm (A) and 405 nm (B) excitation wavelength.

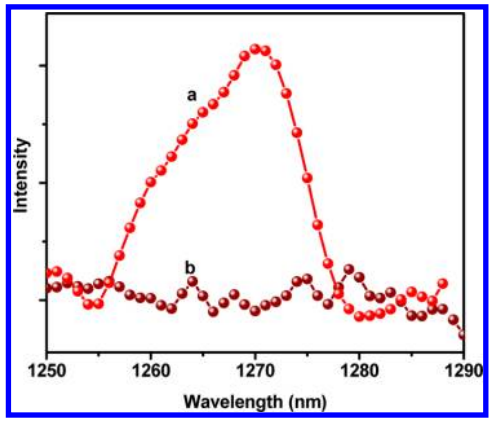

Figure 6. Phosphorescence emission spectra of singlet oxygen for C153-doped PVK with (a) and without (b) surface-attached RB dye molecules.

RB molecules. The PL band at 400 nm is observed for PVK nanoparticles after 340 nm excitation (Figure 3a). The efficient PL quenching (>90%) of host PVK NP is observed in the presence of encapsulated C153 dye molecules (Figure 3b). The PL quenching of PVK polymer nanoparticles is found to be 60%, whereas 1.5 wt % RB dye molecules are attached on the surface of pure PVK NP at 340 nm wavelength of excitation (Figure 3c). After attachment of RB dye molecules on the surface of C153-dye-encapsulated PVK NP, complete quenching of PVK emission is observed. In addition, the emission quenching at 490 nm (due to the encapsulated C153 dye molecules) is found to be 70% (Figure 3d). This PL quenching is mainly due to the efficient energy transfer from PVK nanoparticles to photosensitizer. The possible energy transfer pathways are (a) from host PVK to encapsulated C153 dye molecules, (b) from PVK nanoparticles to surface attached RB dye molecules, (c) from encapsulated C153 dye molecules to surface-attached RB dye molecules, and (d) the overall FRET cascade from PVK to surface-attached RB dye molecules through C153 dye molecules, where C153 can serve as an intermediate energy ladder for funneling the overall exciton energy.

Time-Resolved Spectroscopy. Time-resolved spectroscopic study has been undertaken to elucidate the above-mentioned phenomena. Figure 4 shows normalized emission decay curves of PVK polymer NPs in different conditions. In all cases, we have directly excited the PVK NP at 340 nm excitation. For PVK polymer NP, the emission decay follows multiexponential kinetics including one faster component (0.28 ns) and two comparatively slower components (3.31 and 16.24 ns). The faster component originates from the $\pi-\pi^*$ electronic transition of the conjugated backbone, whereas the slower components are due to the excimeric interactions in nanoparticle form.[35] After surface attachment of 1.5 wt % RB dye molecules on PVK polymer nanoparticles, the decay time of all these components are noticeably shorter (depicted in Table 1). The faster component of the decay changes more effectively (from 280 to 160 ps) with respect to the other two slower components. The average decay time of PVK polymer NPs is

Table 2. Emission Decay Parameters of C153 Encapsulated in PVK NP in Different Conditions

sample	λ_{ex} (nm)	λ_{em} (nm)	τ_1 (ns) a_1	τ_2 (ns) a_2	τ_3 (ns) a_3	<τ> (ns)
C153-doped PVK NP	340	490	0.65 (rise)	6.28 (0.93)	13.4 (0.07)	6.78
C153-doped PVK NP + RB	340	490	3.43 (0.64)	5.95 (0.33)	16.25 (0.03)	4.17
C153-doped PVK NP	405	490	2.16 (0.35)	6.32 (0.65)		4.86
C153-doped PVK NP + RB	405	490	0.011 (0.22)	1.05 (0.27)	4.03 (0.50)	2.35

dx.doi.org/10.1021/jp4127094 | J. Phys. Chem. C 2014, 118, 9733−9740

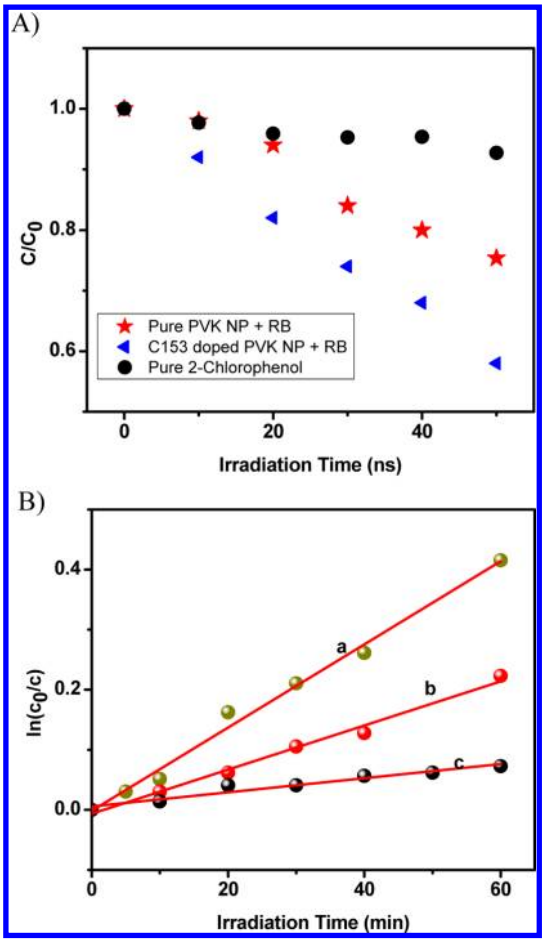

Figure 7. (A) Plot of C/C_0 vs irradiation time for different systems. (B) Plot of $\ln(C/C_0)$ vs irradiation time for (a) C153-doped PVK NP + RB, (b) PVK NP + RB, and (c) pure 2-chlorophenol.

reduced from 1.01 to 0.40 ns in the presence of surface-attached RB dye molecules (by using eq 2). It indicates the efficient FRET process from PVK polymer nanoparticles to surface-attached RB dye molecules. Energy transfer efficiencies in all cases are measured by using the following equation:[32]

$$\phi_{ET} = 1 - \frac{\tau_{DA}}{\tau_D} \quad (4)$$

where τ_{DA} and τ_D are the decay times of polymer nanoparticles in presence and absence of acceptor particles. The energy transfer efficiency from PVK nanoparticles to surface-attached 1.5 wt % RB dye molecules is 60%. However, in the case of 0.8 wt % C153-doped PVK polymer nanoparticles, the average decay of PVK reduced to 0.11 ns from 1.01 ns, indicating the efficient energy transfer phenomena (~90%) from PVK to encapsulated C153 dye molecules. In this particular situation, all the components (slower and faster components) are reduced significantly due to the close proximity of all the donor chromophoric units toward acceptors molecules inside the polymeric nanoparticle matrix. Interestingly, when RB dye molecules are attached with C153-encapsulated PVK polymer nanoparticles, both the slower components of PVK are unchanged with respect to C153-doped system. The faster component is reduced from ~100 ps to ~60 ps, indicating that the exciton energy generated from semiconducting polymer moiety (PVK) cannot directly transfer toward surface-attached RB dye molecules. It clearly suggests that the generated exciton energy transfers from host PVK molecules toward the surface-attached RB dye molecules through the encapsulated C153 dye molecules.

For further clarification, we have measured the emission decay of encapsulated C153 dye molecules with and without surface attached RB dye molecules. Figure 5A clearly shows a 650 ps rise time of encapsulated C153 (excited at 340 nm (i.e., PVK host) and measured at 490 nm, the emission band of C153), which clearly indicates the energy transfer process from host PVK to encapsulated C153 dye molecules. Irrespective of the rise time, we have observed the two decay components, which are 6.28 ns (93%) and 13.4 ns (7%), respectively, at 340 nm excitation wavelength for encapsulated C153 dye molecules. Multicomponent decay of encapsulated dye molecules supports the heterogeneous environments inside polymer nanoparticles.[36] The rise time of C153 disappears in the presence of surface-attached RB dye molecules, and the average decay time of C153 reduces from 6.78 to 4.17 ns, which confirms the energy funneling from C153 to RB at the excitation of PVK host (340 nm). All decay times data are shown in Table 2. To verify the location of C153 after the surface attachment of RB on the polymer NP surface, time-resolved anisotropic study has been undertaken. The time-resolved anisotropy curve of C153 inside the PVK NP remains unaltered after the surface attachment of the RB dye molecule on PVK NP (see Supporting Information Figure S7). It confirms that C153 molecules experience the similar restricted environment inside PVK NP before and after the surface attachment of RB dye molecules.

In addition, time-resolved spectroscopy has also been undertaken to unveil the direct energy transfer process from encapsulated C153 to RB dye molecules. In this context, we have chosen the excitation wavelength of 405 nm, which is the direct excitation of encapsulated C153 dye molecules. Figure 5B shows the normalized emission decay of C153-doped PVK polymer nanoparticles with and without surface-attached RB dye molecules. The average lifetime of C153 encapsulated in PVK nanoparticle is 4.86 ns, and it reduces to 2.35 ns in the presence of surface-attached RB dye molecules. It indicates the direct energy transfer process from encapsulated C153 dye molecules to RB dye molecules. The energy transfer efficiency from encapsulated C153 to RB dye molecules is ~50% (using eq 4) at the direct excitation of encapsulated C153. The corresponding photoluminescence spectra (see Supporting Information Figure S6) again support the direct energy transfer from encapsulated C153 to surface-attached RB dye molecules. The above discussion clearly suggests that the multistep energy transfer process from host PVK to surface-attached RB dye molecules and the direct energy transfer from encapsulated C153 to surface-attached RB dye molecules occur. It reveals that the cascaded energy transfer process occurs from host PVK to surface-attached RB dye molecules through encapsulated C153 dye molecules in polymeric nanoparticles.

Photosensitization and Singlet Oxygen Generation. The above-mentioned study has raised the possibility of generating singlet oxygen from polymer−photosensitizer conjugates. Photoexcited RB undergoes intersystem crossing from the first excited singlet state (S_1) to the tiplet state (T_1) by a nonradiative relaxation process. The triplet state of RB eventually transfers energy nonradiatively toward the triplet oxygen molecules ($^3O_2$) and converts to the singlet oxygen ($^1O_2$) molecules.[37] The photogenerated $^1O_2$ has been investigated by the phosphorescence spectra at the IR region,

dx.doi.org/10.1021/jp4127094 | J. Phys. Chem. C 2014, 118, 9733−9740

Scheme 1. Schematic Representation of Different Pathways of Singlet Oxygen Generation

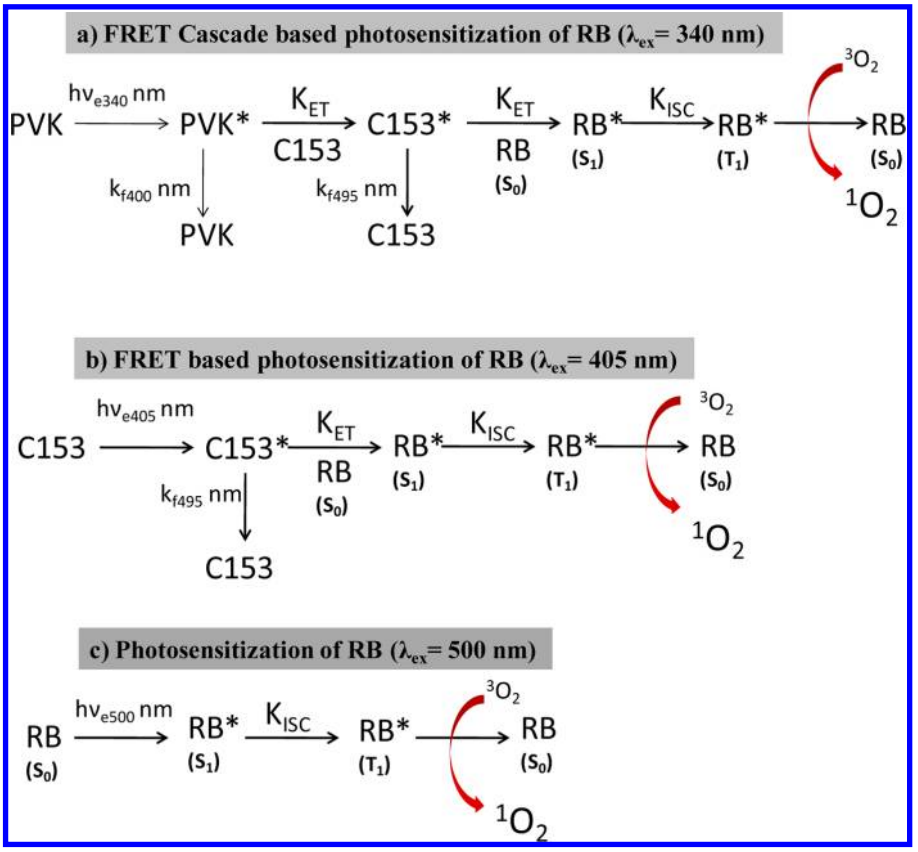

which actually occurs due to radiative relaxation of $^1O_2$. Figure 6 shows the phosphorescence spectra of singlet oxygen at 340 nm excitation wavelength for C153-doped PVK NP with and without surface-attached RB dye molecules in D_2O media. We have observed an emission band in the 1270 nm region upon 340 nm wavelength of excitation in the case of RB-attached C153-doped PVK polymer nanoparticles.[38] However, there is no characteristic emission band for C153-doped PVK polymer nanoparticles. Therefore, a multistep FRET process (PVK → C153 → RB) would help to photosensitize RB dye molecules to generate $^1O_2$ in solution. Due to lack of instrumental facility, we cannot measure the phosphorescence lifetime of singlet oxygen. Furthermore, we have investigated the effect of dopant dye molecules (C153) inside the polymer nanoparticles on the photosensitization of RB dye molecules as well as $^1O_2$ generation in terms of photo-oxidation of 2-chlorophenol in D_2O media. Very recently, Miller and his co-workers demonstrated the photo-oxidation of 2-chlorophenol in the presence of immobilized *meso*-tetraphenylporphyrin.[39] They have reported the interaction of 2-chlorophenol with singlet oxygen after the photosensitization of porphyrin derivatives. Figure 7A describes the concentration change of 2-chlorophenol upon photoirradiation in the case of PVK and RB-attached PVK polymer nanoparticles (C153-doped and undoped). At higher pH, 2-chlorophenol converts to phenolate anion, which reacts faster with singlet oxygen. Therefore, we have adjusted pH 7 to minimize the interaction rate of 2-chlorophenol with photogenerated singlet oxygen. The apparent photo-oxidation rate constant of 2-chlorophenol in the presence of singlet oxygen follows the under-mentioned equation (depicted in Figure 7B)[39]

$$\ln\left(\frac{C_0}{C}\right) = k_{obs}t \tag{5}$$

C_0 and C represent the initial concentration of 2-chlorophenol and at time t, respectively. K_{obs} describes the apparent photo-oxidation rate constant of 2-chlorophenol. For C153-encapsulated PVK nanoparticles (surface-attached RB), K_{obs} is 6.9×10^{-3} s^{-1}. This value reduces to 2.6×10^{-3} s^{-1} without C153. Surprisingly, the apparent photo-oxidation rate is noticeably higher (11.83×10^{-3} s^{-1}) in the case of pure RB in solution. Upon addition of NaN_3 and imidazole, the photo-oxidation rate of 2-chlorophenol reduced to 95% for RB-attached C153-doped PVK polymer nanoparticles. It confirms that the maxium probability of photo-oxidation of 2-chlorophenol is due the photogenerated $^1O_2$ in solution. The singlet oxygen quantum yield for RB-attached C153-doped PVK polymer nanoparticles is 21%, whereas it reduces to 13% for the RB-attached pure PVK nanoparticles system. The quantum yield of singlet oxygen is calculated indirectly from the photo-oxidation of 2-chlorophenol in D_2O medium by using the following equation[40]

$$\Phi_{y0} = \Phi_{ys}(k_s/k_r)(A_r/A_s) \tag{6}$$

where "Φ_{yo}" and "Φ_{ys}" define the singlet oxygen quantum yield of the sample and reference, respectively. Here, we have used RB in D_2O medium as reference, and the singlet oxygen quantum yield for RB in D_2O medium is 0.76. The variables k_s and k_r define the rate of photo-oxidation of 2-chlorophenol by sample and reference dye, respectively. A_r and A_s define the amount of light absorbed by the reference and the sample, respectively. Because the optical density is an additive quantity, the amount of light absorbed should be proportional with the

dx.doi.org/10.1021/jp4127094 | J. Phys. Chem. C 2014, 118, 9733−9740

integrated area of the absorption spectrum as well as the oscillator strength for optical transition.[32]

The higher quantum yield of singlet oxygen in RB-attached C153-doped polymer nanoparticles is due to multiple photosensitization processes. The possible pathways are (a) FRET-cascade-based photosensitization of RB from the host PVK chromophoric unit through encapsulated C153 dye molecules at 340 nm excitation wavelength, (b) direct FRET process from encapsulated C153 dye molecules to surface-attached RB at 405 nm excitation wavelength, and (c) direct excitation of surface-attached RB at ∼500 nm excitation wavelength. Therefore, different wavelengths of excitation can be used for photosensitization of RB dye molecules. All these are depicted in Scheme 1. All these three photosensitization processes have a pronounced effect on the overall singlet oxygen generation in this particular system. Thus, this present fundamental investigation demonstrates the FRET cascade process and multistep energy transfer phenomena based on a fluorophore-doped benign semiconducting polymeric nanodomain. The effect on the photosensitization of RB dye molecules should enrich us for future development of material research regarding photodynamic therapy, blood sterilization, cell biology, and so on.

CONCLUSION

In conclusion, we have successfully synthesized semiconductor polymer nanoparticles−photosensitizer conjugates, which can generate singlet oxygen via a FRET cascade process. The detailed mechanism for generation of singlet oxygen via multistep energy transfer processes has been understood by steady-state and time-resolved spectroscopy. It reveals that the energy migration occurs from PVK host to RB dye molecules via C153 dye, and the singlet oxygen quantum yield is found to be 21%. The present fundamental spectroscopic investigation should further advance the field of material research because of the potential applicability of nanoparticles−photosensitizer conjugates in photodynamic therapy and several theranostics devices.

ASSOCIATED CONTENT

Supporting Information

Figure S1 shows the FE-SEM images of dye-doped PVK NP without and in the presence of RB, Figure S2 shows the zeta potential data, Figure S3 shows the DLS data, Figure S4 shows the UV and PL spectra of RB molecules without and with PVK NP, Figures S5 and S6 represent the additional PL spectra at 340 and 405 nm excitation wavelength. Figure S7 represents the anisotropy decay curves of C153 encapsulated in PVK NP without and in the presence of RB on surface. This material is available free of charge via the Internet at http://pubs.acs.org.

AUTHOR INFORMATION

Corresponding Author

*E-mail: msap@iacs.res.in. Fax: (91)-33-2473-2805. Tel.: (91)-33-2473-4971.

Notes

The authors declare no competing financial interest.

†A.B. worked as a summer student in the laboratory.

ACKNOWLEDGMENTS

SERB (Department of Science and Technology; DST) and Indo-Spain (DST) are gratefully acknowledged for financial support. S.B. and M.B. thank CSIR for awarding a fellowship.

REFERENCES

(1) Celli, J. P.; Spring, B. Q.; Rizvi, I.; Evans, C. L.; Samkoe, K. S.; Verma, S.; Pogue, B. W.; Hasan, T. Imaging and Photodynamic Therapy: Mechanisms, Monitoring, and Optimization. *Chem. Rev.* **2010**, *110*, 2795−2838.

(2) Morris, R. L.; Azizuddin, K.; Lam, M.; Berlin, J.; Nieminen, A.; Kenney, M. E.; Samia, A. C. S.; Burda, C.; Oleinick, N. L. Fluorescence Resonance Energy Transfer Reveals a Binding Site of a Photosensitizer for Photodynamic Therapy. *Cancer Res.* **2003**, *63*, 5194−5197.

(3) Dougherthy, T. J.; Gomer, C. J.; Henderson, B. W.; Jori, G.; Kessel, D.; Korbelik, M.; Moan, J.; Peng, Q. Photodynamic Therapy. *J. Natl. Cancer Inst.* **1998**, *90*, 889−905.

(4) Allen, C. M.; Sharman, W. M.; Van Lier, J. E. Current Status of Phthalocyanines in the Photodynamic Therapy of Cancer. *J. Porphyrins Phthalocyanines* **2001**, *5*, 161−169.

(5) Liu, K.; Liu, X.; Zeng, Q.; Zhang, Y.; Tu, L.; Liu, T.; Kong, X.; Wang, Y.; Cao, F.; Lambrechts, S. A. G.; et al. Covalently Assembled NIR Nanoplatform for Simultaneous Fluorescence Imaging and Photodynamic Therapy of Cancer Cells. *ACS Nano* **2012**, *6*, 4054−4062.

(6) Chen, G.; Yang, C.; Prasad, P. N. Nanophotonics and Nanochemistry: Controlling the Excitation Dynamics for Frequency Up- and Down-Conversion in Lanthanide-Doped Nanoparticles. *Acc. Chem. Res.* **2013**, *46*, 1474−1486.

(7) Holm, B. A.; Bergey, Earl J.; De, T.; Rodman, D. J.; Kapoor, R.; Levy, L.; Friend, C. S.; Prasad, P. N. Nanotechnology in Biomedical Applications. *Mol. Cryst. Liq. Cryst.* **2002**, *34*, 589−598.

(8) Gaponenko, S. V. *Optical Properties of Semiconductor Nanocrystals*; Cambridge University Press: New York, 1998.

(9) Rogach, A. *Semiconductor Nanocrystal Quantum Dots: Synthesis, Assembly, Spectroscopy and Applications*; Springer: New York, 2008.

(10) Samia, A. C. S.; Chen, X.; Burda, C. Semiconductor Quantum Dots for Photodynamic Therapy. *J. Am. Chem. Soc.* **2003**, *125*, 15736−15737.

(11) Hsieh, J. M.; Ho, M. L.; Wu, P. W.; Chou, P. T.; Tsai, T. T.; Chi, Y. Iridium-Complex Modified CdSe/Zns Quantum Dots; A Conceptual Design for Bifunctionality Toward Imaging and Photosensitization. *Chem. Commun.* **2006**, 615−617.

(12) Shi, L.; Billy Hernandez, S.; Hernandez, M. S. B.; Selke, M. Singlet Oxygen Generation from Water-Soluble Quantum Dot-Organic Dye Nanocomposites. *J. Am. Chem. Soc.* **2006**, *128*, 6278−6279.

(13) Tsay, J. M.; Trzoss, M.; Shi, L.; Kong, X.; Selke, M.; Jung, M. E.; Weiss, S. Singlet Oxygen Production by Peptide-Coated Quantum Dot-Photosensitizer Conjugates. *J. Am. Chem. Soc.* **2007**, *129*, 6865−6871.

(14) Charron, G.; Stuchinskaya, T.; Edwards, D. R.; Russell, D. A.; Nann, T. Insights into the Mechanism of Quantum Dot-Sensitized Singlet Oxygen Production for Photodynamic Therapy. *J. Phys. Chem. C* **2012**, *116*, 9334−9342.

(15) Durisic, N.; Bachir, A. I.; Kolin, D. L.; Hebert, B.; Lagerholm, B. C.; Grutter, P.; Wiseman, P. W. Detection and Correction of Blinking Bias in Image Correlation Transport Measurements of Quantum Dot Tagged Macromolecules. *Biophys. J.* **2007**, *93*, 1338−1346.

(16) Tuncel, D.; Demir, H. V. Conjugated Polymer Nanoparticles. *Nanoscale* **2010**, *2*, 484−494.

(17) Pecher, J.; Mecking, S. Nanoparticles of Conjugated Polymers. *Chem. Rev.* **2010**, *110*, 6260−6279.

(18) Mailander, V.; Landfester, K. Interaction of Nanoparticles with Cells. *Biomacromolecules* **2009**, *10*, 2379−2400.

(19) Jin, Y.; Ye, F.; Zeigler, M.; Wu, C.; Chiu, D. T. Near-Infrared Fluorescent Dye-Doped Semiconducting Polymer Dots. *ACS Nano* **2011**, *5*, 1468−1475.

(20) Wu, C.; Zheng, Y.; Szymanski, C.; McNeill, J. Energy Transfer in a Nanoscale Multichromophoric System: Fluorescent Dye-Doped Conjugated Polymer Nanoparticles. *J. Phys. Chem. C* **2008**, *112*, 1772−1781.
(21) Kumar, R.; Ohulchanskyy, T. Y.; Roy, I.; Gupta, S. K.; Borek, C.; Thomson, M. E.; Prasad, P. N. Near-Infrared Phosphorescent Polymeric Nanomicelles: Efficient Optical Probes for Tumor Imaging and Detection. *ACS Appl. Mater. Interfaces* **2009**, *1*, 1474−1481.
(22) Bhattacharyya, S.; Paramanik, B.; Patra, A. Energy Transfer and Confined Motion of Dyes Trapped in Semiconducting Conjugated Polymer Nanoparticles. *J. Phys. Chem. C* **2011**, *115*, 20832−20839.
(23) Wu, C.; Chiu, D. T. Highly Fluorescent Semiconducting Polymer Dots for Biology and Medicine. *Angew. Chem., Int. Ed.* **2013**, *52*, 3086−3109.
(24) Bhattacharyya, S.; Prashanthi, S.; Bangal, P. R.; Patra, A. Photophysics and Dynamics of Dye-Doped Conjugated Polymer Nanoparticles by Time-Resolved and Fluorescence Correlation Spectroscopy. *J. Phys. Chem. C* **2013**, *117*, 26750−26759.
(25) Chen, L. H.; McBranch, D. W.; Wang, H. L.; Helgeson, R.; Wudl, F.; Whitten, D. G. Highly Sensitive Biological and Chemical Sensors Based on Reversible Fluorescence Quenching in a Conjugated Polymer. *Proc. Natl. Acad. Sci. U.S.A.* **1999**, *96*, 12287−12292.
(26) Scholes, G. D. Long-Range Resonance Energy Transfer in Molecular System. *Annu. Rev. Phys. Chem.* **2003**, *54*, 57−87.
(27) Shen, X.; Li, L.; Wu, H.; Yao, S. Q.; Xu, Q. H. Photosensitizer-Doped Conjugated Polymer Nanoparticles for Simultaneous Two-Photon Imaging and Two-Photon Photodynamic Therapy in Living Cells. *Nanoscale* **2011**, *3*, 5140−5146.
(28) Shen, X.; He, F.; Wu, J.; Xu, G. Q.; Yao, S. Q.; Xu, Q. H. Enhanced Two-Photon Singlet Oxygen Generation by Photosensitizer-Doped Conjugated Polymer Nanoparticles. *Langmuir* **2011**, *27*, 1739−1744.
(29) Grimland, J. L.; Wu, C.; Ramoutar, R. R.; Brumaghim, J. L.; McNeill, J. Photosensitizer-Doped Conjugated Polymer Nanoparticles with High Cross-Sections for One- and Two-Photon Excitation. *Nanoscale* **2011**, *3*, 1451−1455.
(30) Bhattacharyya, S.; Sen, T.; Patra, A. Host−Guest Energy Transfer: Semiconducting Polymer Nanoparticles and Au Nanoparticles. *J. Phys. Chem. C* **2010**, *114*, 11787−11795.
(31) Clafton, S. N.; Beattie, D. A.; Vasilev, A. M.; Acres, R. G.; Morgan, A. C.; Kee, T. W. Chemical Defects in the Highly Fluorescent Conjugated Polymer Dots. *Langmuir* **2010**, *26*, 17785−17789.
(32) Lakowicz, J. R. *Principles of Fluorescence Spectroscopy*, 3rd ed.; Kluwer Academic/ Plenum Publishers: New York, 1999; pp 354−464.
(33) Patra, A.; Pan, M.; Friend, C. S.; Lin, T. C.; Cartwright, A. N.; Prasad, P. N.; Burzynski, R. Electroluminescence Properties of Systematically Derivatized Organic Chromophores Containing Electron Donor and Acceptor Groups. *Chem. Mater.* **2002**, *14*, 4044−4048.
(34) Chang, C. C.; Yang, Y. T.; Yang, J. C.; Wu, H. D.; Tsai, T. Absorption and Emission Spectral Shifts of Rose Bengal Associated with DMPC Liposomes. *Dyes Pigm.* **2008**, *79*, 170−175.
(35) Ghosh, D.; Nandi, N.; Chattopadhyay, N. Differential Förster Resonance Energy Transfer from the Excimers of Poly (*N*-vinylcarbazole) to Coumarin 153. *J. Phys. Chem. B* **2012**, *116*, 4693−4701.
(36) Mukherjee, S.; Kombrabail, M.; Krishnamoorthy, G.; Chattopadhyay, A. Dynamics and Heterogeneity of Bovine Hippo-Campal Membranes: Role of Cholesterol and Proteins. *Biochim. Biophys. Acta* **2007**, *1768*, 2130−2144.
(37) Prasad, P. N. *Introduction to Biophotonics*; John Wiley & Sons, Inc.: Hoboken, NJ, 2003; pp 203−249.
(38) Li, B.; Lin, H.; Chen, D.; Wang, Min; Xie, S. Detection System for Singlet Oxygen Luminescence in Photodynamic Therapy. *Chinese Optics Lett.* **2010**, *8*, 86−88.
(39) Gmurek, M.; Mosinger, J.; Miller, J. S. 2-Chlorophenol Photooxidation Using Immobilized Meso-Tetraphenylporphyrin in Polyurethane Nanofabrics. *Photochem. Photobiol. Sci.* **2012**, *11*, 1422−1427.
(40) Lin, H.; Shen, Y.; Chen, D.; Lin, L.; Wilson, B. C.; Li, B.; Xie, S. Feasibility Study on Quantitative Measurements of Singlet Oxygen Generation Using Singlet Oxygen Sensor Green. *J. Fluoresc.* **2013**, *23*, 41−47.